Analog Laser Predistortion for Multiservice Radio-Over-Fiber Systems

L. Roselli, *Senior Member, IEEE*, V. Borgioni, F. Zepparelli, F. Ambrosi, M. Comez, P. Faccin, and A. Casini

***Abstract*—We have developed some low-cost predistortion circuits to compensate second- and third-order laser distortions in multiservice radio-over-fiber industrial systems. Depending on the predistorter configuration implemented, average reductions of 10–15 dB and of 8–10 dB have been observed in the laser second- and third-order distortions, respectively, within the cellular bands relevant to the European TETRA, GSM, and DCS standards. In particular, the development of the prototypes here illustrated is based on a new and original procedure that formalizes and suitably integrates in a sinergistic way modeling, design, and experimental activities.**

***Index Terms*—Compensation, laser modeling, nonlinear distortion, predistortion, radio over fiber (RoF).**

I. Introduction

We describe here the development of low-cost broadband completely analog predistortion circuits used to reduce second- and third-order harmonic distortions (HD2 and HD3) and second- and third-order intermodulations (IM2 and IM3) of semiconductor lasers used in multiservice radio-over-fiber (RoF) industrial systems.

In RoF systems and networks, microwave and millimeter-wave multiplexed signals (briefly, RF signals) modulate an optical carrier generated by a semiconductor laser and are transmitted from a central site through an optical fiber link to the receiver, where a photodetector recovers the original RF information (direct-detection systems). The RF signals can then be distributed to home subscribers, as in the case of cable television (CATV) [1], or radiated to mobile, nomadic, or fixed terminals like in cellular communication networks [2], [3]. Optical beamforming in phased-array antennas [4], [5], signal processing [6], [7], and EM-field remote sensing [8] represent other interesting examples of application of RoF techniques. CATV distribution and GPRS, GSM/DCS, and TETRA microcellular networks are, in particular, the industrial applications for which the study and development of the circuits here illustrated have been committed.

In intensity-modulation direct-detection (IMDD) systems, the intensity of the optical carrier can be directly or externally modulated by immediately driving the laser diode with the RF signal, or with the use of an additional electrooptical modulator, respectively.

The performances of the two solutions are typically comparable up to 10 GHz: the former becomes inefficient over a few tens of gigahertz, mainly due to laser frequency relaxation [9] and chirping [10], [11] combined with the fiber chromatic dispersion [12], but the latter suffers from higher distortion levels, due to the intrinsic nonlinearity of the modulators, and implies higher losses, costs, and complexity. This is the reason why RoF systems based on the direct modulation of semiconductor lasers represent nowadays a more mature and diffused technology for commercial applications.

The performance of a direct IMDD scheme is strongly influenced by the nonlinearity of the laser. When many RF subcarriers are multiplexed together and modulate the light source, harmonic distortions and intermodulation products are generated that influence negatively the quality of the signal at the receiver [3]. If we consider some generic sinusoidal tones f_i, f_j, and f_k as the inputs of a nonlinear device, we will obtain at the output the following frequency components: $mf_i \pm nf_j \pm pf_k$, where m, n, and p are integer numbers that can assume the values 0, 1, 2, ... If two between m, n, and p are simultaneously null, we have the harmonic components of a tone; if at least two of them are different from zero, we talk of intermodulation products. The sum $m + n + p$ defines the order of the harmonics and of the intermodulations; then we can identify second-order harmonic distortion (HD2) $2f_i$, $2f_j$, and $2f_k$; third-order harmonic distortion (HD3) $3f_i$, $3f_j$, and $3f_k$; second-order intermodulation (IM2) $f_i \pm f_j$; and third-order intermodulation (IM3) $2f_i \pm f_j$, $f_i \pm 2f_j$, and $f_i \pm f_j \pm f_k$. Some of these beats fall within the operational band where the original tones are allocated, thus yielding intraband distortion; it is important to note that in those RoF-systems, where the bandwidth of a single laser can be used to allocate several services, there can be an interband negative influence too due to the harmonics or intermodulations that, generated in a certain band, fall within that dedicated to another service.

It should be also underlined that, up to now, fourth and higher orders have been typically considered as negligible because at very low power levels, or well outside the operational bands. However, if the exactness of this assumption can be widely demonstrated by classical CATV applications [1], [13], recent works [14], [15] have pointed out that, especially with systems making use of multicarrier standards like the Universal Mobile Telecommunication System (UMTS), depending on the characteristics of the fiber link and/or of the amplifier adopted, also fifth- and seventh-order products can affect negatively the useful signal. In this paper, we focus our attention mainly on second- and third-order components, due to their strong influence on the

Manuscript received September 30, 2002; revised January 28, 2003.

L. Roselli, F. Zepparelli, and F. Ambrosi are with the Department of Electronic and Information Engineering, University of Perugia, I-06125 Perugia, Italy (e-mail: roselli@diei.unipg.it).

V. Borgioni and M. Comez are with WIS S.r.l., I-06034 Foligno, Italy (e-mail: valeria.borgioni@wis-srl.com).

P. Faccin and A. Casini are with Tekmar Sistemi S.r.l., I-48018 Faenza, Italy (e-mail: pier.faccin@tekmar.it).

Digital Object Identifier 10.1109/JLT.2003.810931

systems taken into consideration; nonetheless, as will be clearer later on, the principles of the approach described here can be extended to include also higher odd-order distortions in view of a more general strategy of compensation.

To ensure a satisfying quality of the services released to the users, it is mandatory to keep the distortions below certain levels. Each service is characterized by its specific standard; for example, analog video signals require distortion levels more than 50 dB below that of the carrier to reach a carrier-to-noise ratio (CNR) around 45 dB and be imperceptible [1], [13]; in GSM picocellular and microcellular networks, a satisfying CNR is given by values of the input dynamic range (DR) varying from 40–55 dB to 80–90 dB, respectively [2]; the UMTS standard requires an adjacent channel leakage power ratio of -45 dBc for the downlink and -33 dBc for the uplink [16], corresponding to values of the DR of about 30 dB. In any case, this implies the realization of highly linear RoF systems. In view of large-scale productions, economical considerations suggest the use of compensated low-cost lasers rather than extremely linear but expensive devices. This implies the resort to compensation techniques that must be low-cost solutions themselves.

There are two major methods to reduce the nonlinear distortions generated by lasers: feedforward compensation and predistortion. The feedforward technique seems to be superior because it also reduces the laser intensity noise [17]; however it has a technoeconomical drawback represented by the fact that it requires a greater number of components such as additional laser diodes, a photodiode, and an optical coupler, resulting in higher costs and complexity of the total system. Predistortion can be a simpler approach since it implies only the insertion of an electronic predistorter somewhere in front of the light source to generate correcting frequency components equal in amplitude, but opposite in phase, to those undesired introduced by the laser nonlinearity. The problem of predistortion can be afforded in several ways. Predistortion blocks can be designed based on Volterra models to invert the light-current characteristic curve of a laser operating in the CATV band up to 500 MHz, thus compensating its nonlinearities [18]. Remarkable results have been obtained with adaptive predistortion: in [19], the compensation of an analog predistortion circuit is maximized through the use of a microcontroller, thus reducing by 20 dB third-order intermodulations over the frequency range 1750 $\div$ 1870 MHz. The same principles can be applied to externally modulated lasers in RoF systems operating around 10 GHz or more [20].

To keep costs and complexity as low as possible, being interested in industrializable prototypes, we have realized some completely analog predistortion circuits able to reduce about 10-dB second- and third-order distortions of an entire class of commercial lasers, in the frequency range 370 $\div$ 1980 MHz, over which CATV channels, up to more than 800 MHz, GPRS, GSM/DCS, and TETRA cellular communication bands can be simultaneously allocated. The predistorters are then virtually suited to multiservice RoF systems, the only limitation being the difference in the output power level typically requested to each service. The development of these preindustrialized prototypes, illustrated through the following sections, is the yield of the sinergy of modeling, design, and experimental activities.

Following the scheme suggested by Sum and Gomes [21], shown in Fig. 1, as a basis for the design of a predistortion circuit and to estimate its compensation capabilities, a laser circuit model has been previously developed and implemented into a commercial software package. In order to realize a predistorter able to correct the nonlinear behavior of an entire class of optical transmitters, a parameter extraction from a lot of four lasers has been performed, thus obtaining a laser circuit model with a sort of average behavior.

The laser modeling and the subsequent parameter extraction procedure are described in Section II.

Once having obtained a satisfying laser model, the next step has been the design of the predistorter. First, a suitable configuration has been selected and implemented; our choice fell on a "three-paths" predistorter reported in [22], suited to correct both second- and third-order distortions. The behavior of such a configuration has been optimized through computer-aided design (CAD) simulations, by exploiting, to this aim, the laser model previously characterized. As a consequence of this CAD activity, a first prototype, suited to work within the aforementioned cellular frequency bands, has been realized and subjected to an extensive experimental characterization. Several single-tone and two-tone tests have pointed out the broadband functionality of the circuit: average 10–15 dB and 8–10 dB compensations of the laser second-order (HD2 and IM2) and third-order (IM3) distortions, respectively, have been observed from the TETRA band (370 $\div$ 480 MHz) up to the DCS band (1710 $\div$ 1980 MHz). However, it is important to note that the overall circuit behavior was not completely satisfying: the nonlinear paths of the predistorter, devoted to compensate second- and third-order distortions, have shown a mutual spurious coupling, an effect not predicted by the CAD, that has practically prevented us from obtaining a simultaneous correction of the different kinds of distortions. Then, such a procedure has been iterated: we have introduced and validated some modifications into the original predistorter configuration at the CAD and realized a new prototype. The first experimental measurements have pointed out that such a new circuit can simultaneously reduce laser HD2, IM2, and IM3 of about 12 dB and 6–8 dB, respectively, within the whole DCS frequency band, thus allowing for the industrialization of the predistorter.

The design and development of these circuits are the subject of Section III.

II. Laser Modelling

As outlined in the Introduction, the first steps toward the realization of the predistorter have been the development and experimental characterization of a semiconductor laser circuit model able to reproduce the behavior of the class of industrial devices to be compensated, namely, thermostabilized distributed feedback (DFB) laser JDS/Uniphase CQF940, with emission wavelength of 1310 nm. Such a model has been implemented into the commercial software package Agilent EEsof EDA Advanced Design System (ADS) and characterized through a parameter extraction procedure from the measurements relevant to a lot of four samples of the abovementioned class.

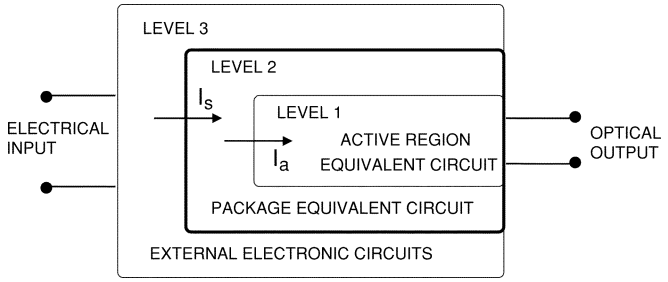

Fig. 1. Block diagram illustrating the multilevel modeling and design approach. $I_{\rm s}$ represents the microwave current (bias-plus-signal) feeding the laser and $I_{\rm a}$ the microwave current injected into the laser active region.

A. Equivalent Circuit

The operational characteristics of a semiconductor laser are described by the *rate equations*, which govern the electron–photon interactions taking place within the optically active region of the device

$$\frac{\partial N}{\partial t} = \frac{I_a}{q v_{\rm act}} - \frac{N}{\tau_n} - g(N - N_0)(1 + \varepsilon_{NL} S)^{-\frac{1}{2}} S \quad (1)$$

$$\frac{\partial S}{\partial t} = \Gamma \beta \frac{N}{\tau_n} - \frac{S}{\tau_p} + \Gamma g(N - N_0)(1 + \varepsilon_{NL} S)^{-\frac{1}{2}} S. \quad (2)$$

N and S are the electron and photon densities, respectively, I_a the injected current, q the electron charge, $v_{\rm act}$ the volume of the active region, τ_n the electron lifetime, g the optical power gain coefficient, N_0 the electron density at transparency, ε_{NL} the optical gain compression parameter, Γ the optical confinement factor, β the probability of radiative spontaneous emission, and τ_p the photon lifetime. The corrective factor $(1 + \varepsilon_{NL} S)^{-1/2}$ models an equivalent saturation of the optical gain; in this way, the effect of the nonuniform distribution of electrons into the active region (lateral diffusion), which has a nonnegligible influence on the dynamic response of the laser, is accounted for along with some other nonlinear effects like spatial and spectral hole burning. This expression has been preferred to the original one $(1 - \varepsilon_{NL} S)$ introduced by Tucker *et al.* [23], [24] since it eliminates the problem of the nonphysical multiple solutions that the model can yield during software simulations when $\varepsilon_{NL} S > 1$. To eliminate such a problem, while keeping an accurate description of the lateral diffusion, Channin [25] proposed the expression $(1+\varepsilon_{NL} S)^{-1}$, always positive. Mena [26] has demonstrated that all the expressions $(1 + \varepsilon_{NL} S)^{-p}$, with $0 < p < 1$, can be used satisfactorily; we have chosen the expression $(1+\varepsilon_{NL} S)^{-1/2}$ originally proposed by Agrawal [27].

By suitably rewriting (1) and (2) in terms of current contributions [28], the large-signal equivalent circuit of the active region can be derived. To describe correctly the behavior of the real device, the effect of the package also has been considered by cascading the aforementioned circuit with another including lumped parasitic elements. The choice of the parasitic circuit is not unique but dependent on the type of the device considered; we have adopted the configuration proposed by Salgado and O'Reilly in [29]. The complete circuit is shown in Fig. 2.

Further equations that explicitate the physical meaning of some parameters have been implemented too [30]. In particular, we have used the following expression that relates the photon lifetime to the laser cavity parameters:

$$\tau_p^{-1} = \frac{c}{n}\left[\alpha + \frac{1}{L} ln\left(\frac{1}{R}\right)\right]. \quad (3)$$

In (3), c is the light velocity in a vacuum, n the refractive index of the material, α the relevant effective optical absorption coefficient, L the cavity length, and R the reflectivity. The volume of the active region has been expressed as the product of the three dimensions

$$v_{\rm act} = L \times W \times d \quad (4)$$

with W and d as the width and the thickness, respectively. The equation relating the density of photons generating the laser radiation to the output optical power has been also included

$$P_{out}^{\rm opt} = \frac{1}{2} \cdot \frac{h\nu S v_{\rm act}}{\tau_{\rm es}} \quad (5)$$

where h is the Planck constant, ν the frequency of the emitted photons, and τ_{es} the relevant escape time from the active region, expressed by the following formula:

$$\tau_{\rm es}^{-1} = \frac{1}{2} \cdot \frac{c}{nL} ln\left(\frac{1}{R}\right). \quad (6)$$

B. Experimental Measurements and Parameter Extraction

One of our goals is to use the predistortion circuitry in order to achieve a good dynamic range for analog and wireless applications using inexpensive coaxial laser devices, even not specifically selected for this kind of application. The other goal is to improve the overall dynamic range performance (including the second- third-order compensation) of analog lasers for high-end wireless applications equipped with thermostabilized laser devices. In order to start with our experiments, as a first approach, we have used a butterfly-packaged temperature-controlled DFB device JDS/Uniphase CQF940, with emission wavelength of 1310 nm. For the sake of statistical significance, a lot of four lasers has been considered and measured. Fig. 3 shows a schematic of the measurement setup used to characterize experimentally the four transmitters.

First, we have determined the light-current characteristic curves of the four devices by the use of an optical power meter, as shown in the right half of Fig. 3. Then, with each device, the frequency dependence of the S-parameters of the RoF link shown in the left side of Fig. 3 has been measured. In this case, short standard single-mode fiber (SMF) cables, having an attenuation factor of 0.4 dB/Km and negligible chromatic dispersion at 1310 nm, have been used, with the optical attenuator simulating a 12.5-km-long fiber link. For the distribution of CATV channels and TETRA, GSM/DCS, GPRS services, the lasers are typically operated below 2 GHz; however, to the aim of getting a fuller characterization of the devices, a frequency range from dc to 5 GHz has been considered. Moreover, to have information on the maximum admissible modulating RF power, the average optical modulation index (OMI) of the lasers has been also measured. Fig. 4 shows that the RF input power had to be kept below 12 dBm.

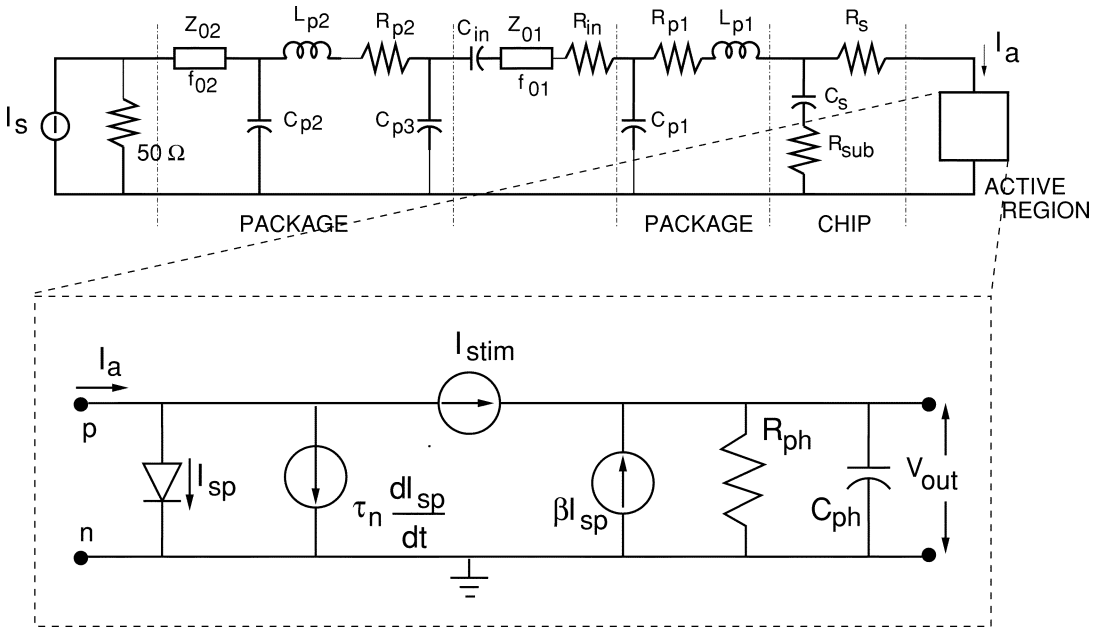

Fig. 2. Complete laser equivalent circuit. For the definition of $I_{\rm sp}$, $I_{\rm stim}$, $\mathrm{R_{ph}}$, $\mathrm{C_{ph}}$, and $\mathrm{V_{out}}$ see [23], [24].

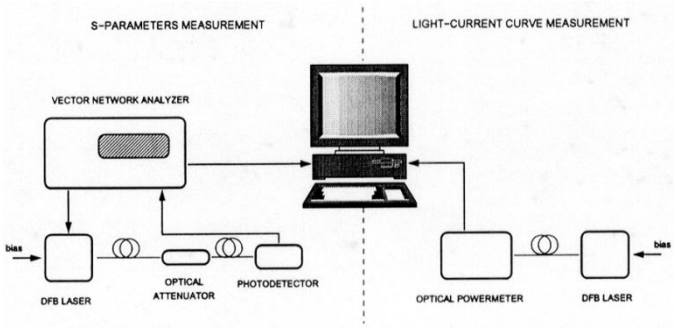

Fig. 3. Measurement setup used to characterize the lot of four lasers considered.

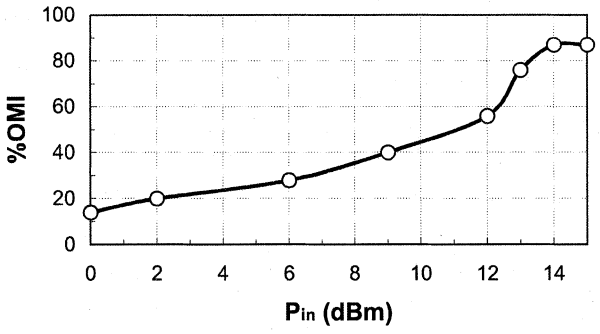

Fig. 4. Average measured laser OMI as a function of the input RF power.

In order to develop an industrializable prototype of the predistortion circuit, we have extracted the laser model parameters from the average curves of the lot. In particular, the procedure we have followed, also with the aid of the optimization routines of ADS, consisted of the following steps.

1) The measured average curves have been given as optimization goals to the simulator.
2) First-guess values have been assigned to the laser package and active region equivalent circuit parameters.
3) The S_{11} microwave coefficient frequency curve, which is almost completely independent of the bias current, has been used to extract the package parameters.
4) The S_{21} microwave coefficient frequency curve, at the bias current $I = 38$ mA, and the light-current curve have been used to extract the active region parameters.
5) Once a first satisfying agreement between measurements and simulations has been obtained, a conclusive fine optimization has been performed by taking into consideration the complete set of the measured curves as optimization goals, simultaneously.

Figs. 5 and 6 show the comparison between measured and simulated average curves at the end of the optimization for two different polarization currents $I_1 = 38$ mA and $I_2 = 50$ mA, respectively; in Table I, the final values of the parameters are listed.

C. Nonlinear Distortion Prediction

With the values of the parameters of Table I, we have first determined the S_{11} and S_{21} frequency curves for different bias currents, always obtaining a good agreement with measurements (these curves are not shown here for the sake of brevity). Then we have tested the ability and accuracy of the model in reproducing the nonlinear behavior of the lasers. As an example of the results obtained, Fig. 7 shows the comparison between predicted and measured HD2 and IM3 curves, averaged over the four devices, at the bias values $I = 38$ mA and $I = 50$ mA.

III. Predistorer Design and Development

Once having obtained an accurate laser circuit model, the following step has been the development of the predistorter. The design and development procedure, consisting of CAD and experimental activities, has been iterated until the realization of a satisfying pre-industrialized prototype, as summarized by Fig. 8.

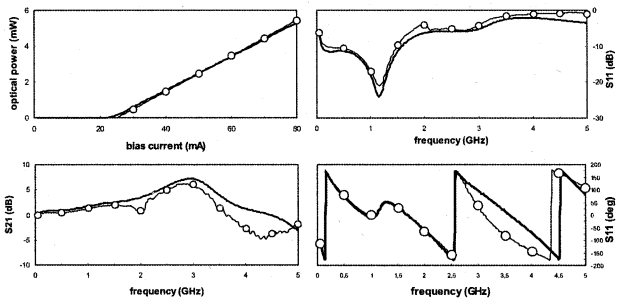

Fig. 5. Laser circuit model parameter extraction $I_1 = 38$ mA: comparison between measurements (circles) and simulations (solid line) after the optimization: (a) light-current curve; (b) S_{21}; (c) S_{11}-modulus; (d) S_{11}-phase.

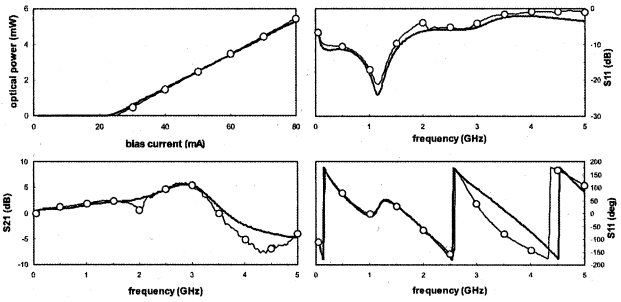

Fig. 6. Laser circuit model parameter extraction $I_2 = 50$ mA: comparison between measurements (circles) and simulations (solid line) after the optimization: (a) light-current curve; (b) S_{21}; (c) S_{11}-modulus; (d) S_{11}-phase.

TABLE I
OPTIMIZED PARAMETER VALUES OF THE LASER CIRCUIT MODEL

PACKAGE	
$Z_{02} = 56.69$ ohm	$f_{02} = 1.12$ GHz
$C_{p2} = 8.30$ pF	$L_{p2} = 0.76$ nH
$R_{p2} = 0.02$ ohm	$C_{p3} = 0.84$ pF
$C_{in} = 91.00$ pF	$R_{in} = 25.30$ ohm
$Z_{01} = 52.93$ ohm	$f_{01} = 2.82$ GHz
$C_{p1} = 6.52$ pF	$R_{p1} = 2.00$ ohm
$L_{p1} = 0.52$ nH	$C_s = 6.43$ pF
$R_{sub} = 3.09$ ohm	$R_s = 4.28$ ohm
ACTIVE REGION	
$L = 239.66$ μm	$W = 3.11$ μm
$d = 0.34$ μm	$n = 3.62$
$N_0 = 1.67 \times 10^{+24}\mathrm{m}^{-3}$	$g = 6.01 \times 10^{12}\mathrm{m}^3\mathrm{s}^{-1}$
$\beta = 3.79 \times 10^{-03}$	$\Gamma = 0.43$
$\varepsilon_{NL} = 5.0 \times 10^{-23}\mathrm{m}^3$	$\alpha = 951.20\ \mathrm{m}^{-1}$
$R = 0.29$	$\tau_n = 3.40$ ns

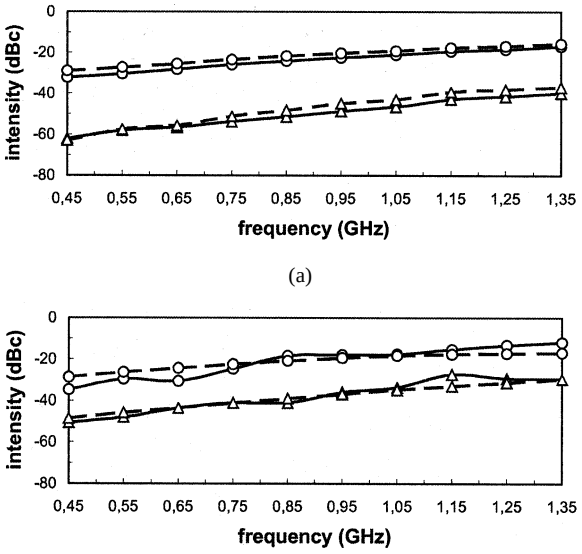

Fig. 7. (a) Laser HD2 and (b) IM3 product $2f_1 - f_2$: comparison between measured (solid line) and predicted (dashed line) curves of two typical values of the bias current, $I = 38$ mA (circles) and $I = 50$ mA (triangles). Input sinusoidal tones with an RF power of 3 dBm have been used in both cases. For the intermodulation, f_1 is variable and $f_2 = 815$ MHz.

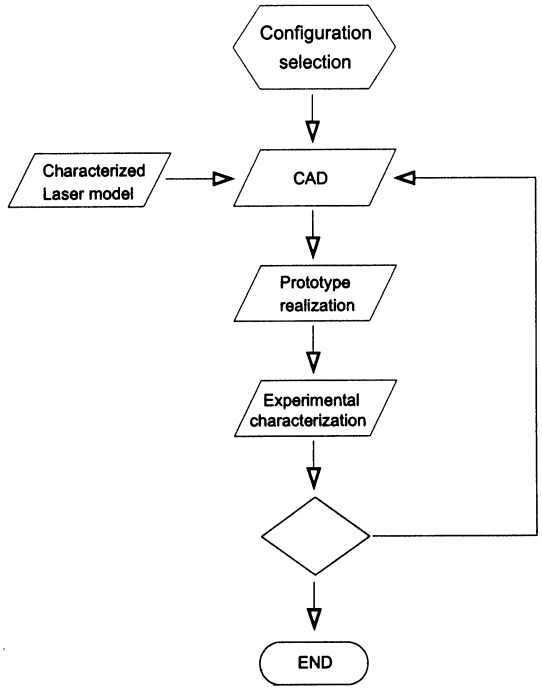

Fig. 8. Predistorter design and development procedure.

A. First Prototype: CAD

The solution adopted has been derived from a predistorter configuration presented in [22] and shown in Fig. 9. It is possible to identify two main parts: a linear part and a nonlinear part. The former simply consists of a time delay line, while the latter is further subdivided into second-order and third-order paths. Portions of the input RF signal are extracted to feed both quadratic-law (X^2) and cubic-law (X^3) generators. The two correction signals, with magnitude and phase suitably adjusted through a chain of shaping blocks, are then recombined with the original delayed RF signal and sent to the laser. In this way, the circuit can simultaneously compensate HD2, HD3, IM2, and IM3 distortions.

Fig. 9 also suggests the possibility to extend the compensation capability of this configuration simply by inserting higher order paths and thus correcting, where needed, further sets of distortions, as for example the aforementioned fifth- and seventh-order IMs in UMTS systems.

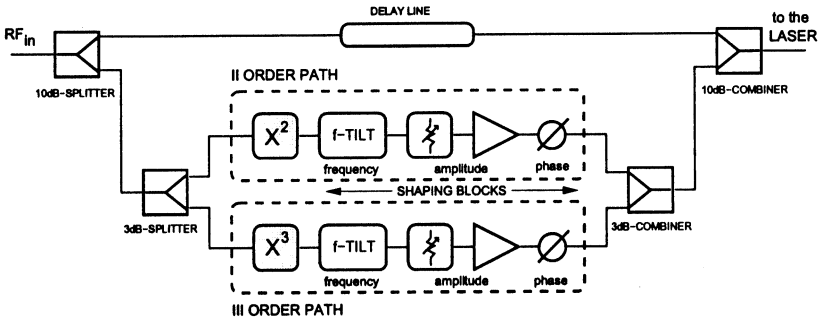

Fig. 9. Schematic diagram of the first predistorter prototype.

To feed and recombine the linear and nonlinear paths of the predistorter, 10- and 3-dB splitters/combiners have been implemented.

The quadratic-law device can be realized with a couple of diodes in push–push configuration, fed with two 180° shifted inputs. To have a large operational frequency range, a differential amplifier has been used to realize the input phase shift. The cubic-law device can also be realized with a couple of diodes, but in push–pull configuration and with no input phase shift [31].

The function of the shaping chains is to generate correction signals having the same magnitudes but opposite phases, with respect to the laser nonlinearities, in a frequency range as wide as possible. To this aim, two low-noise amplifiers (LNAs) have been inserted after the nonlinear generators to adjust the magnitude level of the drawn correction signals, which suffer an overall attenuation of about 30 dB due to the input and output splitters and combiners; a fine control on the magnitude level has been assured by variable attenuators. Also a fine phase-adjustment stage, to match the laser harmonic phase variations, has been inserted in both the nonlinear paths. Finally, frequency-tilt shaping networks have been implemented to let the correction signals match the laser distortion curves in the whole operational band. In practice, these are equalization filters, realized by variable lumped passive components, having a frequency response that has to be suitably adjusted to follow exactly the tilt in the laser harmonic distortion frequency curves. In this way, the correction band can be maximized and the same configuration of the predistorter can be adapted to different laser classes or periodically retuned to prevent the variations due to the laser aging. Concerning this point, it has to be noted that there are several undesired effects that can cause differences in the behavior of devices part of the same class. Along with the abovementioned laser aging, which gradually alters in time the light power emitted, there can be a temperature-dependent shift of the threshold current; everything is then furtherly complicated by manufacturing tolerances that produce parameter values spreading.

If the last aspect is generally the most difficult to face, several techniques are available to minimize the temperature effects and the laser aging. At present, there exist laser devices, as those taken into consideration in this paper, that are thermostabilized so as to practically eliminate such a problem: obviously this solution implies higher costs. Alternatively, one can resort to simpler and cheaper, not stabilized, devices and design the ancillary circuitry (like the predistorter, in this case) by inserting the temperature-dependence effect into the laser model used [32]. A similar scenario can be depicted for laser aging prevention: an automatic power control loop, enabled by an external photodiode, can be used to maintain constant average optical output power over laser-aging variations; to avoid cost enhancements, one can accept the laser aging while counteracting it with a programmed retuning of the electronic circuitry, for example, through the periodical regulation of the control voltages for the phase shifters and attenuators.

The laser model, as identified in Section II, has been cascaded to the predistorter described above and the whole subsystem simulated. Fig. 10 summarizes the second-order distortion compensation procedure and the relevant results: first the correction signal has been suitably shaped in magnitude and phase, exploiting the HD2 curves of the laser, over the whole operational band, as shown in (a) and (b); then the HD2 and IM2 generation of the predistorted laser has been compared with that of the uncompensated laser. An average reduction of about 10 dB in both (c) and (d) curves can be observed in the frequency range $0.4 \div 2$ GHz. It is important to remark here that the broadband compensation of the HD2 yields automatically the optimum compensation of the IM2 too, since both distortions are generated by second-order nonlinearities with comparable magnitude levels. The same considerations hold only partly for third-order distortions: in fact, the correction signal, after being shaped with the aid of the HD3 curves, has to be afterwards adjusted in magnitude to yield the maximum compensation of the IM3 products. In particular, this is due to the fact that IM3-difference products are typically generated with magnitude levels different from those of the HD3, and such a trend remains verified until the frequency spacing of the components forming the IM3 product is not very wide [12]. Fig. 11 shows the relevant results.

B. First Prototype: Realization and Experimental Characterization

Based on the CAD results illustrated up to now, the first prototype of the predistorter shown in Fig. 12 has been realized. The configuration implemented has a simple architecture; most of its components have cheap commercial counterparts; and no digital or adaptive technique is used.

Even if the broadband functionality predicted by simulations pointed out the possibility of using a single predistorter for both

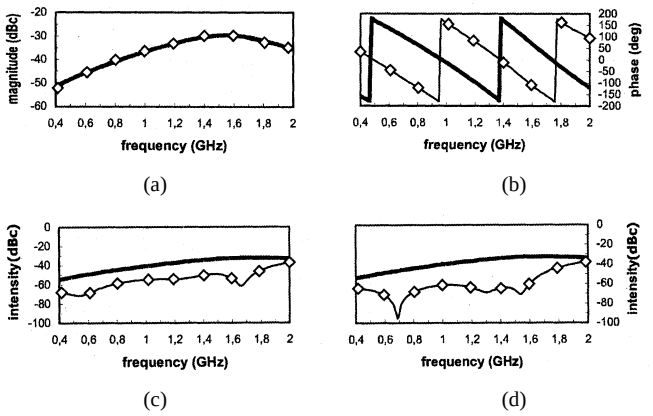

Fig. 10. Laser second-order compensation: higher graphs illustrate the shaping of the correction signal (diamonds), (a) magnitude and (b) phase, performed using the laser HD2 curves (solid line); lower graphs show a comparison between compensated (diamonds) and uncompensated (solid line) (c) HD2 and (d) IM2 product $f_1 + f_2$. Input sinusoidal tones with an RF power of 3 dBm have been used in both cases.

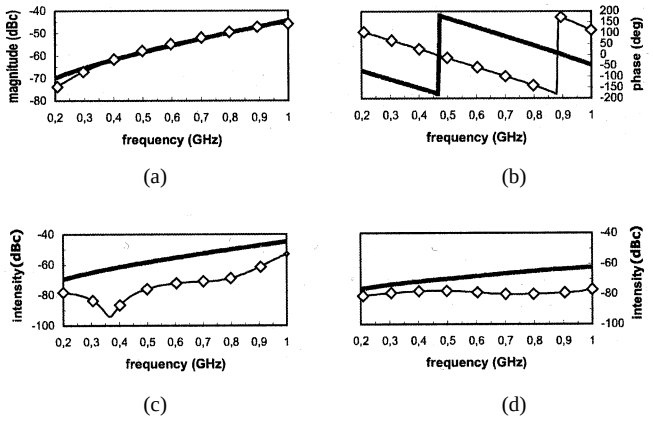

Fig. 11. Laser third-order compensation: higher graphs illustrate the shaping of the correction signal (diamonds), (a) magnitude and (b) phase, performed using the laser HD3 curves (solid line); lower graphs show a comparison between compensated (diamonds) and uncompensated (solid line) (c) HD3 and (d) IM3 product $2f_1 - f_2$. Input sinusoidal tones with an RF power of 3 dBm have been used in both cases.

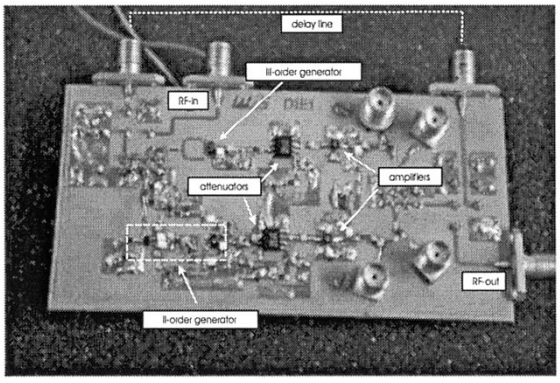

Fig. 12. First prototype of the predistorter.

CATV and cellular communications, the difference among the power levels typical of the two breeds of service has forced us to specialize the circuit for one of them. The prototype then has been realized with the aim of improving the quality of service in TETRA, GSM/DCS, and GPRS RoF networks.

The prototype has been subjected to an extensive experimental characterization; several single-tone and two-tone tests have been performed to check the effectiveness of the compensation. Fig. 13 shows the relevant measurement setup. Single-tone tests have been performed by means of the harmonic measurement tool of a network analyzer HP 8753, whose output tone, suitably filtered and with a 12-dBm RF power, fed the predistorter. The cascaded laser to be compensated has been biased with a current of 51 mA; since about 3 dB are lost through the predistorter, the actual RF power entering the laser was 9 dBm, a value corresponding to an OMI of about 40%, as can be seen in Fig. 4. The optical attenuator has been set to simulate again a 12.5-km-long fiber link. The HD2 and HD3 frequency curves have been finally recorded by the network analyzer.

For two-tone tests, the RF input signals have been yielded by the use of two frequency-tone generators and sent to the predistorter via a duplexer; two circulators have been used to isolate the generators. A spectrum analyzer by Rohde–Schwarz has recorded the intermodulation products as a function of the input RF power. In both cases, a final data processing has been performed by a PC.

As already pointed out, the main problems arise with the second- and third-order distortions generated by the laser. Fig. 14 summarizes the situation relevant to the cellular bands considered.

DCS and GSM bands are negatively influenced by HD2- and IM2-sum products generated in GSM and TETRA bands, respectively. IM2-difference products can fall within GSM and TETRA bands when due to the beat of DCS-GSM and GSM-TETRA frequency components, respectively.

HD3- and IM3-sum products do not represent a problem, as can be seen in Fig. 14; third-order distortion is mainly due to interband IM3-difference products.

Concerning the compensation procedure, to minimize interband second-order distortions falling, e.g., in GSM band, it is fundamental to shape the magnitude of the relevant correction signal so as to follow the laser HD2 frequency curve due to the fundamental component in a band that could be defined as GSM/2, almost corresponding to the TETRA band; at the same time, the phase opposition has to be also achieved in the same band. To correct second-order distortions in DCS band, the same procedure has to be followed by considering the GSM band as the "shaping-band."

Similarly, to minimize intraband third-order distortions falling, for example, in GSM band, a suitable shaping on the laser HD3 is needed; however, in this case, the GSM/3 shaping-band does not coincide with the TETRA band. Based on the abovementioned considerations, the following measurement sessions have been performed to characterize the predistorter.

- II ORDER PATH
  1) Session—Figs. 15 and 16: the TETRA band has been considered as the shaping-band to compensate HD2, IM2-sum, and IM2-difference products in the 740 ÷ 960 MHz band, containing the GSM band; the test tones were: $f_1 = 450$ MHz and $f_2 = 460$ MHz for the HD2 and IM2-sum, and

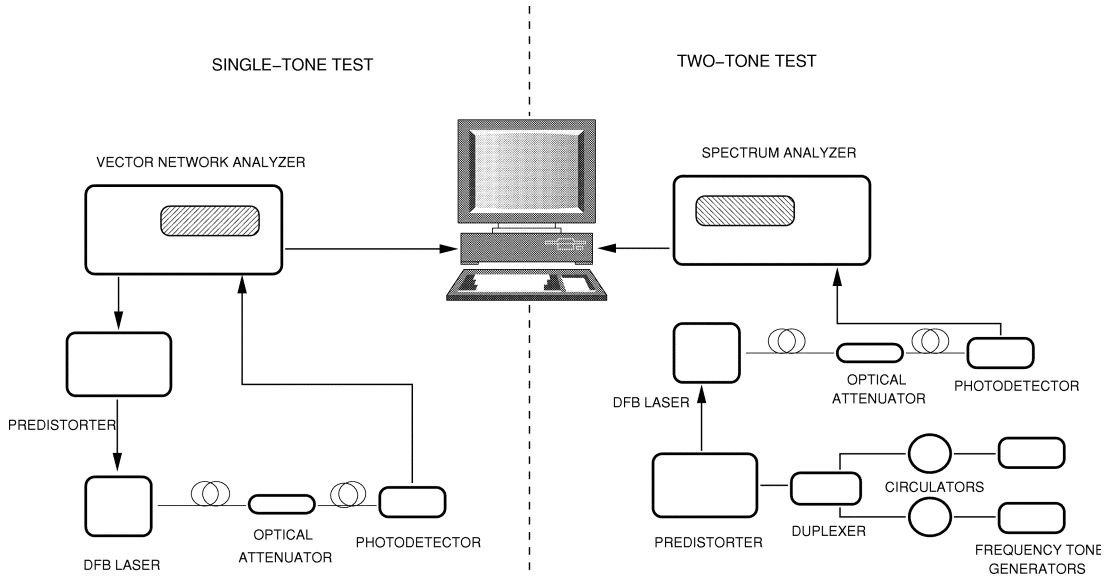

Fig. 13. Measurement setup used to characterize the first predistorter prototype.

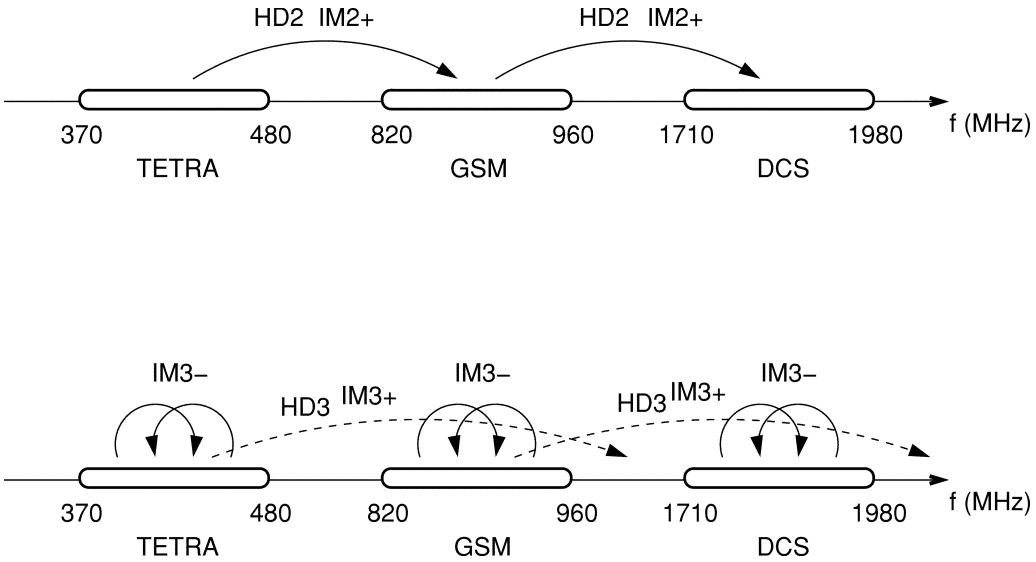

Fig. 14. Influence of the second-order (higher graph) and third-order (lower graph) distortions among and within the cellular bands.

$f_3 = 1850$ MHz and $f_4 = 930$ MHz for the IM3-difference.

2) Session—Figs. 17 and 18: the $560 \div 960$ MHz band, containing the GSM band, has been considered as the shaping-band to compensate HD2 and IM2-sum products in the $1120 \div 1920$ MHz band, containing the DCS band; the test tones were: $f_1 = 900$ MHz and $f_2 = 930$ MHz.

- III ORDER PATH

1) Session—Figs. 19 and 20: the $260 \div 360$ MHz band, containing the GSM/3 band, has been considered as the shaping-band to compensate IM3-difference products in the $780 \div 1080$ MHz band, containing the GSM band; the test tones were: $f_1 = 900$ MHz and $f_2 = 930\ hboxMHz$.

Even if the CAD does not give any indication about possible spurious coupling between the two nonlinear paths of the predistorter, it seemed reasonable to forecast such an undesired effect. Then, first of all, we have decided to characterize the two cor-

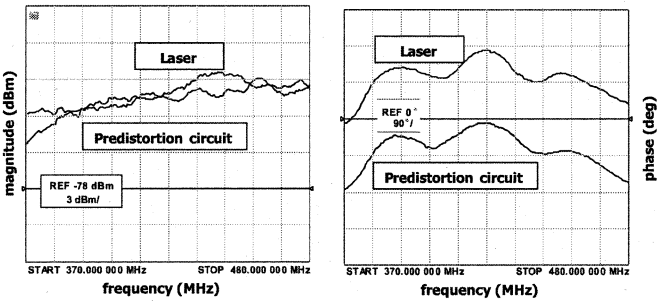

(a) (b)

Fig. 15. First predistorter prototype—second-order path measurement session n.1: shaping of the (a) magnitude and (b) phase of the correction signal within the TETRA band.

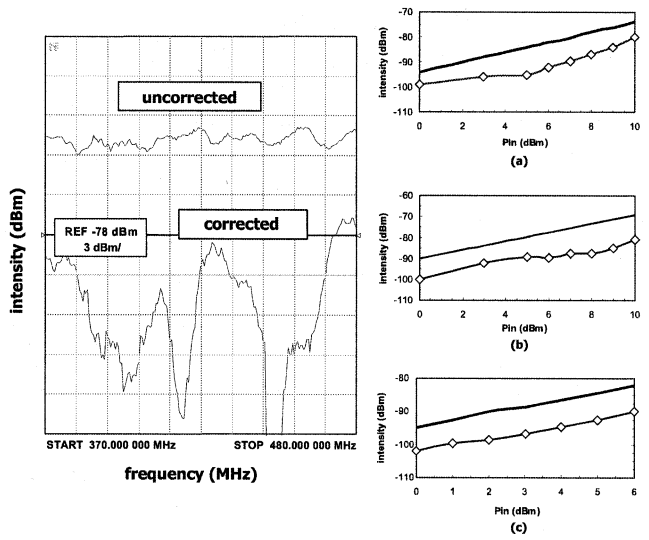

Fig. 16. First predistorter prototype—second-order path measurement session n.1—laser compensation in 740 ÷ 960 MHz band, containing the GSM band: (left) HD2 frequency curve; (right) HD2 (a) $2f_1$, (b) IM2-sum product $f_1 + f_2$, and (c) IM2-difference product $f_4 - f_3$.

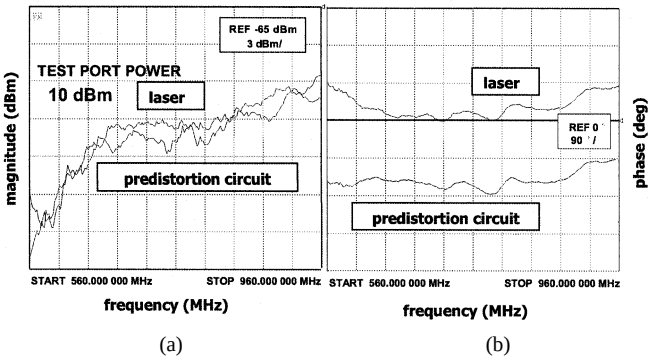

Fig. 17. First predistorter prototype—second-order path measurement session n.2: shaping of the (a) magnitude and (b) phase of the correction signal in 560 ÷ 960 MHz band, containing the GSM band.

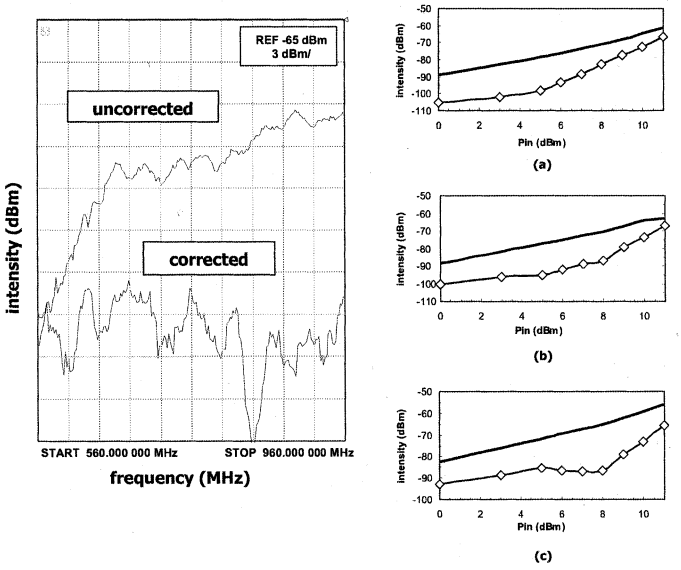

Fig. 18. First predistorter prototype—second-order path measurement session n.2—laser compensation in 1120 ÷ 1920 MHz band, containing the DCS band: (left) HD2 frequency curve; (right) (a) HD2 $2f_1$, (b) HD2 $2f_2$, (c) IM2-sum product $f_1 + f_2$.

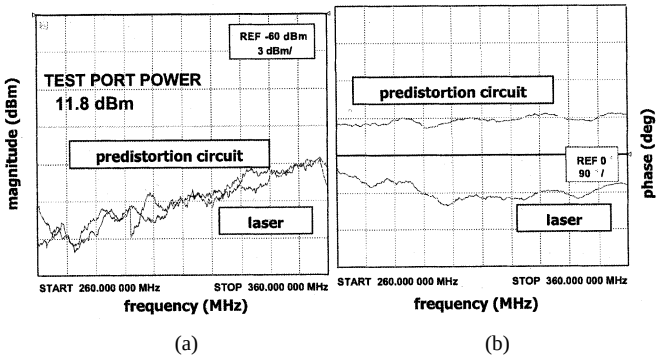

Fig. 19. First predistorter prototype—third-order path measurement session n.1: shaping of the (a) magnitude and (b) phase of the correction signal in 260 ÷ 360 MHz band, containing the GSM/3 band.

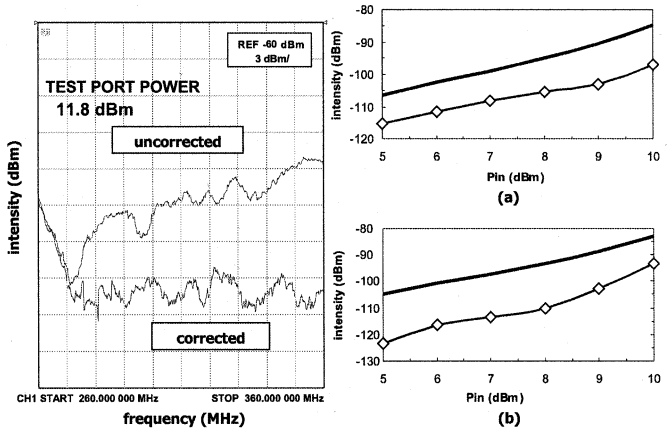

Fig. 20. First predistorter prototype—third-order path measurement session n.1—laser compensation in 780 ÷ 1080 MHz band, containing the GSM band: (left) HD3 frequency curve; (right) IM3-difference product (a) $2f_1 - f_2$ and (b) $2f_2 - f_1$.

rection paths separately, also to point out the relevant maximum performance.

It is necessary at this point to comment on the results obtained. First, it has to be pointed out that with the compensation procedure performed, we have observed an average reduction of about 10 dB of HD2 and IM2 in the GSM band, 12 ÷ 15 dB of HD2 and IM2 in the DCS band, and 9 ÷ 10 dB of IM3 in the GSM band. The same degree of third-order distortion correction can be obtained also in the TETRA and DCS bands, even if the relevant results are not shown here for the sake of brevity.

Another important feature of the predistorter to underline is the checked possibility of correcting second-order distortions both in GSM and DCS bands with only one shaping performed in the 560 ÷ 960 MHz band (containing the GSM band), in other words without resorting to the further shaping in the TETRA band.

In this way, what was already introduced in [12] and observed, in the present case, during the CAD phase has found a new experimental confirmation.

Nevertheless, the first prototype, when used with the two correction paths acting simultaneously, has shown a critical coupling. In fact, the spurious second-order component generated by the amplification stage in the third-order path and the spurious third-order component due to the nonideal rejection of the

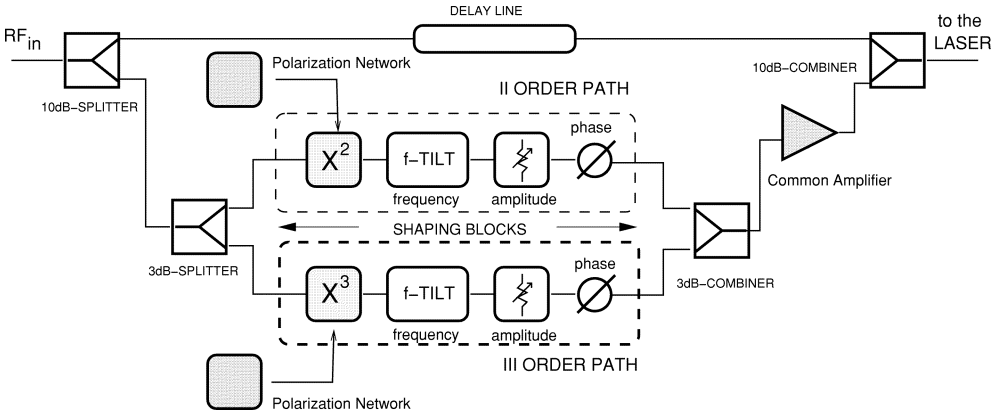

Fig. 21. Modified predistorter schematic.

quadratic-law generator in the second-order path (see Fig. 9), deteriorate the correction capabilities of the circuit.

However, although our final goal is the realization of a predistorter able to reduce second- and third-order laser distortions simultaneously, the results obtained cannot be considered completely negative. It is, in fact, indubitable that each one of the correction paths can be implemented by itself to obtain two different predistorters devoted to correct a certain order of distortion; moreover, the experimental characterization shows that the relevant behaviors are really broadband and multiservice.

C. Final Prototype

To solve the problem of the mutual coupling between the correction paths, the predistorter configuration of Fig. 9 has been suitably modified by inserting two polarization networks for the nonlinear generators and by replacing the two LNAs of the nonlinear paths with a common amplification stage placed after the output 3-dB combiner, as shown in Fig. 21.

The polarization of the diodes has been foreseen to increase both the spurious harmonics rejection and operating transduction, simultaneously. The use of a single common amplifier stage, specifically designed to have maximum linearity, together with a power consumption reduction, allows for a better lineup of the whole system in terms of linearity, thus reducing further the generation of undesired distortion components.

This new configuration has been studied at the CAD, and the new prototype shown in Fig. 22 has been realized and measured to validate the changes.

The same setup shown in Fig. 13 has been used for a new experimental characterization. The compensation procedure already illustrated in the previous section has been repeated. The magnitude and phase frequency curves of the second-order correction signal have been shaped with the aid of the laser HD2 curves in the 500 ÷ 960 MHz band, containing the GSM band; for the third-order correction signal, the laser HD3 curves have been considered in the 500 ÷ 660 MHz band, containing the DCS/3 band. In this way, a simultaneous reduction of the laser HD2- and IM2-sum, about 10–12 dB, and IM3-difference, about 6–7 dB, over the whole DCS band has been obtained, as shown by Figs. 23 and 24. Also in this case, it is foreseeable that the frequency range where the second-order distortions are effectively corrected can be extended at least down to the whole GSM band.

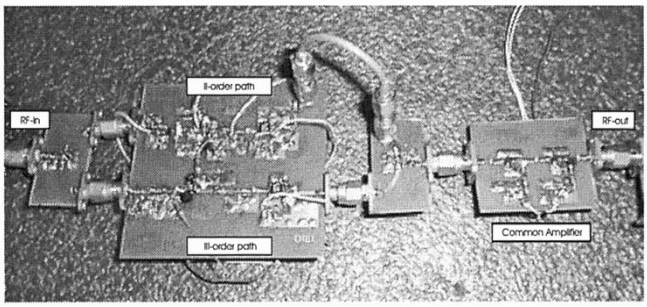

Fig. 22. Picture of the second prototype of the predistorter.

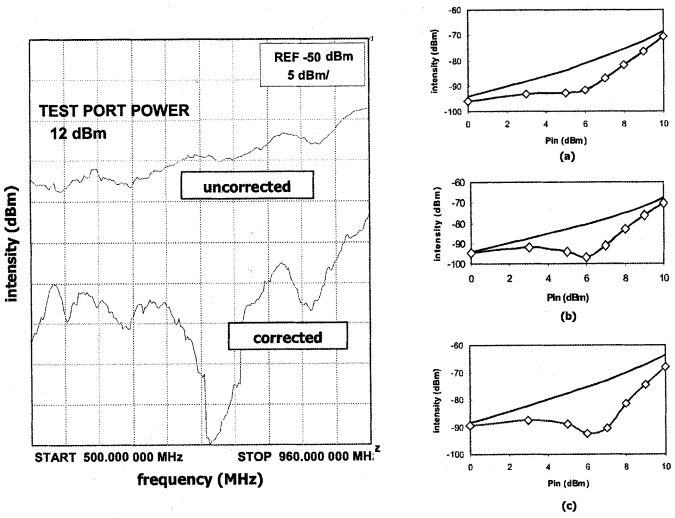

Fig. 23. Final predistorter prototype—laser second-order compensation in 1000 ÷ 1920 MHz band, containing the DCS band: (left) HD2 frequency curve; (right) (a) HD2 $2f_1$, (b) HD2 $2f_2$, (c) IM2-sum product $f_1 + f_2$.

On the contrary, for the third-order distortions, a tradeoff between the simultaneous functionality and the operational bandwidth of the predistorter has been observed: even if not shown here, a similar correction within the TETRA and GSM bands has not been possible. This effect is still dependent on the spurious harmonics due to the nonlinear generators (diodes), while the amplifier has no more influence, having been placed after the nonlinear paths. The diode residual harmonic generation increases almost linearly with the frequency; below the DCS band, its level becomes comparable with that of the laser HD3, which,

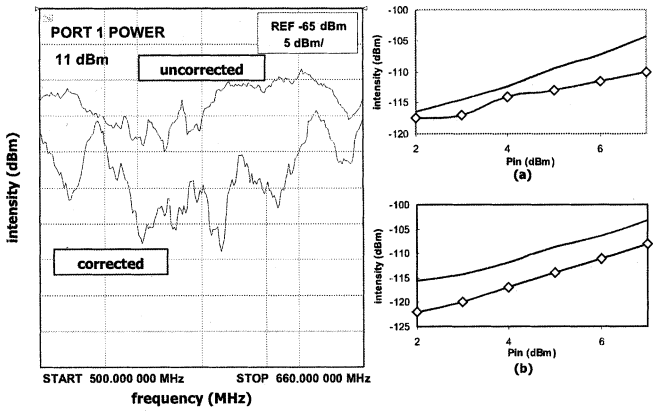

Fig. 24. Final predistorter prototype—laser third-order compensation in 1500 ÷ 1980 MHz band, containing the DCS band: (left) HD3 frequency curve; (right) (a) IM3-difference product $2f_1 - f_2$, (b) IM3-difference product $2f_2 - f_1$.

on the contrary, increases with the frequency as the third power; thus, moving down the spectrum, the shaping of the third-order path correction signal is always more and more difficult, until becoming impossible. Such a problem does not arise for the second-order path correction signal because the laser HD2, used for the shaping, has a level always sufficiently higher than the residual spurious floor.

IV. Conclusion

In this paper, some predistortion circuits for RoF cellular systems, working with the European TETRA, GSM, and DCS standards, have been presented. The design of the various prototypes here illustrated is strongly oriented to industrial applications; thus it refers to low-cost, completely analog solutions for large-scale productions. The configurations implemented are based on simple architectures, where most of the simulated components have cheap commercial counterparts and no digital or adaptive technique is used. Although predistortion is a well-estabilished linearization technique, this paper has pointed out, experimentally, some original aspects worth to be noted. In particular, a new, complete, and original design procedure for RoF systems has been introduced and formalized.

The abovementioned design procedure involves first of all the development and full characterization of a laser circuit model. The laser model reported here has been characterized through a parameter extraction procedure, performed by taking into consideration the measurements relevant to four samples of the same class of DFB lasers. In particular, it has been verified that such a model describes in a satisfying way the nonlinear behavior of the real devices. This result has been obtained without referring to the nonlinear curves for the optimization, thus having a further proof of its accuracy and effectiveness. An extraction of the parameters based on the nonlinear curves too allows for a further refinement of the model, but it is also more complicated and time-consuming. If needed, the dependence on the temperature of the laser emission can be quite easily included into the model. This has not been done in this paper due to the fact that we have considered thermostabilized devices. The model can be also modified to describe the behavior of different laser configurations.

Among the other design steps, particularly interesting, in the authors' opinion, is the predistorter tuning procedure, set up at the CAD and subsequently performed and optimized experimentally. Such a procedure, which is mainly based on the positive use of the same laser distortions to be compensated, has given us a deeper comprehension of the nonlinear phenomena influencing RoF communications and, in point of fact, has led to the implementation of effective predistorter prototypes.

Concerning the various circuits, the first predistorter realized is a "three-path" configuration able to compensate alternatively second- or third-order harmonic and intermodulation distortions generated by the nonlinear behavior of the laser. A spurious mutual coupling between the two correction paths, mainly due to the RF components, has prevented the simultaneous compensation of the laser HD2, IM2, and IM3. Nevertheless, as confirmed by the measurements performed, such a configuration can be the basis for the development of two different broadband and multiservice predistorters specifically devoted to reduce one breed of distortion. By iterating the design procedure, some modifications to the original configuration have been investigated at the CAD and introduced to realize a new prototype. As a result, a preindustrialized predistorter capable of reducing simultaneously the laser HD2- and IM2-sum of about 10–12 dB, and IM3-difference of about 6–7 dB, over the whole DCS band has been obtained.

Finally, but as already explained, RoF systems based on the UMTS standard were beyond the scope of this paper and thus they have not been examined. However, the approach and the techniques here illustrated can be naturally extended to the UMTS field. If the main problems arise from second- and third-order distortions up to 2.1-GHz operational bands, the same predistorter configurations can be used with a new selection of components, always more and more available for third-generation (3G) applications, and retuning of the circuitry. On the other side, to include the compensation of higher odd-order distortions, the same architecture introduced here, with a suitable selection of the devices needed to realize fifth- and seventh-order nonlinear generators, and of the electronic components forming the relevant shaping chains, can be the basis for "multipath" predistorter configurations. Obviously, the price to pay is an increasing complexity of the circuits and during the design procedure, but in view of a future wide expansion of 3G-communication systems and networks, to the authors' opinion the development of a low-cost compensation technique remains a solution worth pursuing and an interesting research opportunity.

Acknowledgment

The authors would like to thank Giuseppe Fabiano (Medeos) and Taconic for the provision of the dielectric substrates used in the fabrication of the prototypes.

References

[1] J. A. Chiddix, H. Laor, D. M. Pangrac, L. D. Williamson, and R. W. Wolfe, "AM video on fiber in CATV systems: need and implementation," *IEEE J. Select. Areas Commun.*, vol. 8, pp. 1229–1239, Sept. 1990.

[2] W. I. Way, "Optical fiber-based microcellular systems: an overview," *IEICE Trans. Commun.*, vol. E76-B, pp. 1091–1102, Sept. 1993.

[3] O. K. Tonguz and H. Jung, "Personal communications access networks using subcarrier multiplexed optical links," *IEEE J. Lightwave Technol.*, vol. 14, pp. 1400–1409, June 1996.
[4] I. Frigyes and A. J. Seeds, "Optically generated true-time delay in phased-array antennas," *IEEE Trans. Microwave Theory Tech.*, pt. II, vol. 43, pp. 2378–2386, Sept. 1995.
[5] W. Freude, G. Chakam, and V. Hurm, "Microwave photonics for broadband wireless access," in *Proc. Photonics '98, IIT Delhi*, Dec. 14–18, 1998, pp. 217–222.
[6] D. Dolfi *et al.*, "Optical architectures for programmable filtering and correlation of microwave signals," *IEEE Trans. Microwave Theory Tech.*, pt. II, vol. 45, pp. 1467–1472, Aug. 1997.
[7] S. Tedjini, A. Ho-Quoc, and D. A. M. Khalil, "All-optical networks as microwave and millimeter-wave circuits," *IEEE Trans. Microwave Theory Tech.*, vol. 43, pp. 2418–2434, Sept. 1995.
[8] R. Heinzelmann *et al.*, "Optically powered remote optical field sensor system using an electroabsorption modulator," in *1998 IEEE MTT-S Dig.*, Baltimore, MD, June 7–12, 1998, pp. 1225–1228.
[9] R. G. Hunsperger, *Integrated Optics—Theory and Technology*, 4th ed. Berlin, Germany: Springer-Verlag Telos, Oct. 1995.
[10] W. E. Stephens and T. R. Joseph, "System characteristics of direct modulated and externally modulated RF fiberoptic links," *IEEE J. Lightwave Technol.*, vol. LT-5, p. 380, 1987.
[11] C. Cox III, E. Ackermann, R. Helkey, and G. E. Betts, "Techniques and performance of intensity-modulation direct-detection analog optical links," *IEEE Trans. Microwave Theory Tech.*, pt. II, vol. 45, pp. 1375–1383, Aug. 1997.
[12] C. S. Ih and W. Gu, "Fiber induced distortions in a subcarrier multiplexed lightwave system," *IEEE J. Select. Areas Commun.*, vol. 8, pp. 1296–1303, Sept. 1990.
[13] Lucent Technologies, System analysis, component selection and testing consideration for 1310 nm analog fiber-optic CATV applications, in Application Note, June 1998.
[14] R. Schuh, D. Wake, and E. Sundberg, "A simple linearity analysis for active distributed antenna systems using W-CDMA signals," in *Int. Top. Meeting Microwave Photonics Tech. Dig. (MWP'01)*, Long Beach, CA, Oct. 7–10, 2001.
[15] S. Hunziker, "Low-cost fiber optic links for cellular remote antenna feeding," in *Radio Over Fiber Technologies for Mobile Communication Networks*, H. Al-Raweshidy and S. Komaki, Eds. Boston, MA: Artech House, 2002.
[16] R. Schuh and D. Wake, "Distortion of W-CDMA signals over optical fiber links," in , *Int. Top. Meeting Microwave Photonics Tech. Dig. (MWP'99)*, Melbourne, Australia, Nov. 17–19, 1999, pp. 9–12.
[17] L. Fock, A. Kwan, and R. S. Tucker, "Reduction of semiconductor laser intensity noise by feedforward compensation: experiment and theory," *IEEE J. Lightwave Technol.*, vol. 10, pp. 1919–1925, Dec. 1992.
[18] N. Tayebi and M. Kavehrad, "Laser nonlinearity compensation for radio subcarrier multiplexed fiber optic transmission systems," *IEICE Trans. Commun.*, vol. E76-B, no. 9, pp. 1103–1114, Sept. 1993.
[19] G. Steiner, S. Hunziker, and W. Baechtold, "Reduction of 3rd order intermodulation of a semiconductor laser by an adaptive low-cost predistortion circuit at 1.8 GHz," in *Proc. 1999 IEEE/LEOS Top. Meeting RF Photonics for CATV and HFC Systems*, San Diego, CA, July 26–30, 1999.
[20] L. Zhang *et al.*, "Ten-GHz MMIC predistortion circuit for improved dynamic range of broadband analog fiber-optic link," *Microwave Opt. Technol. Lett.*, vol. 11, no. 6, pp. 293–295, Apr. 1996.
[21] K. C. Sum and N. J. Gomes, "Microwave-optoelectronic modeling approaches for semiconductor lasers," *Proc. Inst. Elect. Eng. Optoelectron.*, vol. 145, no. 3, pp. 141–146, June 1999.
[22] M. Nazarathy, C. H. Gall, and C. Kuo, "Predistorter for high frequency optical communication devices," U.S. Patent 5 424 680, 1995.
[23] R. S. Tucker and I. P. Kaminow, "High-frequency characteristics of directly modulated InGaAsP ridge waveguide and buried heterostructures lasers," *IEEE J. Lightwave Technol.*, vol. LT-2, pp. 385–393, Aug. 1984.
[24] R. S. Tucker and D. J. Pope, "Circuit modeling of the effect of diffusion on damping in a narrow-stripe semiconductor laser," *IEEE J. Quantum Electron.*, vol. QE-19, pp. 1179–1183, July 1983.
[25] D. J. Channin, "Effect of gain saturation on injection laser switching," *IEEE J. Appl. Phys.*, vol. AP-50, pp. 3858–3860, June 1979.
[26] P. V. Mena, S. Kang, and T. A. DeTemple, "Rate-equation-based laser models with a single solution regime," *IEEE J. Lightwave Technol.*, vol. 15, pp. 717–730, Apr. 1997.
[27] G. P. Agrawal, "Effect of gain and index nonlinearities on single-mode dynamics in semiconductor lasers," *IEEE J. Quantum Electron.*, vol. 26, pp. 1901–1909, Nov. 1990.
[28] R. S. Tucker, "Large-signal circuit model for simulation of injection-laser modulation dynamics," *Proc. Inst. Elect. Eng.*, pt. I, vol. 128, no. 5, pp. 180–184, Oct. 1981.
[29] H. M. Salgado and J. J. O'Reilly, "Experimental validation of Volterra series nonlinear modeling for microwave subcarrier optical systems," *Proc. Inst. Elect. Eng. Optoelectron.*, vol. 143, no. 4, pp. 209–213, Aug. 1996.
[30] W. I. Way, "Large signal nonlinear distortion prediction for a single-mode laser diode under microwave intensity modulation," *IEEE J. Lightwave Technol.*, vol. LT-5, pp. 305–315, Mar. 1987.
[31] W. Huang and R. E. Saad, "Novel third-order distortion generator with residual IM2 suppression capabilities," *IEEE Trans. Microwave Theory Tech.*, vol. 46, pp. 2372–2381, Mar. 1998.
[32] P. V. Mena, "Circuit-level modeling and simulation of semiconductor lasers," PhD dissertation, Univ. of Illinois at Urbana-Champaign, 1998.

L. Roselli (SM'01), photograph and biography not available at the time of publication.

V. Borgioni received the Laurea degree (in electronic engineering from the University of Perugia, Perugia, Italy, in 2001.

Since 2001, she has collaborated with the University of Perugia in the area of predistortion and linearization techniques in radio-over-fiber telecommunication apparatuses and mean power amplifiers. Since June 2002, she has worked as a Design Engineer at WiS s.r.l in Foligno, Italy. Her current interests are the in the area of radio frequency telecommunication systems and linearization techniques.

F. Zepparelli received the Laurea and Ph.D. degrees in electronic engineering from the University of Perugia, Perugia, Italy, in 1998 and 2001, respectively.

Since 2000, he has been a tutor of the Microwaves course for the telecommunication engineering diploma at the University of Perugia. In 2002, he was with the Department of Electronic and Information Engineering (DIEI) of the University of Perugia, where he was a Contract Researcher. Since the beginning of 2003, he has been with the Technical Division of the Town Hall of the City of Perugia, Italy, working in the area of technological infrastructures. His research interests have been connected with the modeling of optical waveguides, lasers, and microwave/photonic devices, mainly oriented to the development of radio-over-fiber systems. His recent publications cover the development of radio frequency predistortion techniques for laser transmitters.

F. Ambrosi received the Laurea degree in electronic engineering from the University of Perugia, Perugia, Italy, in 2000.

Since 2000, he has been with the Department of Electronic and Information Engineering (DIEI) of the University of Perugia, working on the modeling and design of predistortion techniques for radio-over-fiber optical transmitters. Currently, he is with Sirti S.p.a., Milan, Italy, working on the design and deployment of cellular communication networks.

M. Comez received the Laurea degree in electronic engineering from the University of Perugia, Perugia, Italy, in 1999.

Since 1999, he has collaborated with the University of Perugia in the development and design of microwave circuits for transmission of data stream telemetry and of predistortion and linearization techniques. From August 2000 to January 2002, he was an Associate of the WiS S.r.l. society, where he was a Project Manager in radio frequency area circuits for wide-band telecommunications applications. Since January 2002, he has been the WiS President.

P. F. Faccin received the Laurea degree in electronic engineering from the University of Bologna, Bologna, Italy, in 1986.

He was then a Fellow Researcher at Fondazione Guglielmo Marconi, Bologna, Italy, working on modal converters for corrugated waveguides. During the military service, he was involved in measurements of aero–naval moving targets in the Radar Cross Section of the Italian Navy Research Laboratory "G. Vallauri," Livorno, Italy. He was then employed at the Research and Development Division of Telettra, Chieti, Italy, working on military spread-spectrum radio communications. Since 1998, he has been with Tekmar Sistemi S.r.l., where he is responsible for the Core Research Department.

A. Casini was born on November 30, 1956 in Rome, Italy. After achieving the high-school diploma in humanistic disciplines in Rome, in 1975, he attended the telecommunication engineering course at State University of Engineering, Bologna, Italy, from 1975 to 1980.

He developed his first technical skills in amateur radio since 1970 (I4SJX). During his studies he wrote several technical articles on radio communications and was responsible for technical infrastructure at local radio stations. In 1980, as a radio frequency (RF) and microwave Design Engineer, he developed, in cooperation with Philips Semiconductors, an innovative solide-state, high-efficiency RF power amplifier for broadcast FM radio transmitters; he was also involved in designing phase-locked loop frequency synthesizers and other parts of radio transmitters and communication equipment, including antennas. From 1985 to 1987, he developed fiber-optic multichannel video and data communication systems. From 1988 to 1990, he was responsible for developing innovative solutions in microwave transmission links for video and sound, deployed for quick roll-out regional extensions of broadcasting networks. He co-founded Tekmar Sistemi S.r.l., Faenza, Italy, in 1991, bringing with him his experience from 13 years as a radio communications professional in research and development and project management. He is currently President and Managing Director of Tekmar. Since founding Tekmar and until 1996, when the company joined Allen Telecom, he led both the Research and Development and Marketing departments. From 1994 to 1995, he supported standardization activities at ETSI SMG2 for GSM. Currently, he personally supports 3G standardization initiatives at 3GPP RAN.